Cooling and Autonomous Feedback in a Bose-Hubbard Chain with Attractive Interactions

S. Hacohen-Gourgy,[1,*] V. V. Ramasesh,[1] C. De Grandi,[2] I. Siddiqi,[1] and S. M. Girvin[2]
[1]Quantum Nanoelectronics Laboratory, Department of Physics, University of California, Berkeley, California 94720, USA
[2]Departments of Physics and Applied Physics, Yale University, New Haven, Connecticut 06520, USA
(Received 25 June 2015; published 9 December 2015)

We engineer a quantum bath that enables entropy and energy exchange with a one-dimensional Bose-Hubbard lattice with attractive on-site interactions. We implement this in an array of three superconducting transmon qubits coupled to a single cavity mode; the transmons represent lattice sites and their excitation quanta embody bosonic particles. Our cooling protocol preserves the particle number—realizing a canonical ensemble—and also affords the efficient preparation of dark states which, due to symmetry, cannot be prepared via coherent drives on the cavity. Furthermore, by applying continuous microwave radiation, we also realize autonomous feedback to indefinitely stabilize particular eigenstates of the array.

DOI: 10.1103/PhysRevLett.115.240501 PACS numbers: 03.67.Ac, 03.67.Pp, 05.30.Jp, 05.50.+q

Ordinarily, uncontrolled dissipation destroys quantum coherence, but it is now appreciated that an engineered quantum bath is a valuable resource for quantum computation (state preparation [1–4] and system reset [5]) and quantum error correction [6]. A dynamical bath can induce cooling or heating, and is of great utility in opto-mechanical ground state preparation [7,8], quantum state transfer between various EM modes [9–11], amplification [12–14], many-particle quantum simulation [15,16], and entanglement generation [17,18].

Initially conceived and implemented in trapped ion systems [19,20], dissipation engineering has been implemented in solid state systems with two recent experiments on superconducting qubits: autonomously controlling the orientation on the Bloch sphere of a single qubit [3], and stabilizing a Bell state in a two-qubit system [4]. In this Letter, we experimentally demonstrate that dissipation engineering can be used to control a novel, complex superconducting system embodying a much larger Hilbert space: the ten lowest-lying energy levels of a coupled, three-transmon array which realizes a one-dimensional, attractive Bose-Hubbard Hamiltonian. The techniques employed in this work define a path for cooling and stabilizing complex quantum systems to specific target states.

The Bose-Hubbard Hamiltonian [21] is a prototypical model used to describe a broad class of quantum matter. While the repulsive side of the Bose-Hubbard phase diagram has been extensively explored in groundbreaking experiments with ultracold atoms in optical lattices [22–24], the attractive regime has thus far eluded emulation. Our realization of this model here, in perhaps its simplest incarnation, opens the door to experimental verification of as-yet unexplored predictions of attractive Bose-Hubbard dynamics: the existence of self-bound states [25–27] and the possibility to create large-scale multipartite entanglement [28].

The cooling protocol we develop here, based on Raman scattering processes, facilitates entropy and energy exchange between the qubit array and its bath while preserving the total number of excitation quanta in the array. Essentially, this amounts to simulation within the canonical ensemble; a similar path to grand-canonical simulation via bath engineering (using photons) has recently been proposed theoretically by Hafezi *et al.* [29]. In another related work, a cooling scheme similar to ours has been employed recently to measure the dynamic structure factor of a gas of cold atoms [30]. Additionally, a recent experiment with superconducting qubits has achieved simulation of the unitary Fermi-Hubbard dynamics via discrete gates [31].

Our system is comprised of an array of three capacitively coupled transmon qubits [32], each coupled dispersively [33] to a waveguide cavity [34]. The two qubits on the ends of the array utilize a SQUID loop to allow tuning their frequencies via an external magnetic field. Taking into account the full transmon spectrum [32], the system is described by the Hamiltonian $H = H_{\mathrm{cav}} + H_{\mathrm{array}} + H_{\mathrm{int}}$, with

$$H_{\mathrm{cav}} = \hbar\omega_c(a^\dagger a + 1/2), \tag{1}$$

$$\begin{aligned} H_{\mathrm{array}} = {} & \hbar\sum_{j=1}^{3}\left(\omega_j b_j^\dagger b_j + \frac{\alpha_j}{2} b_j^\dagger b_j^\dagger b_j b_j\right) \\ & + \hbar J\sum_{j=1}^{2}(b_{j+1}^\dagger b_j + b_j^\dagger b_{j+1}) \\ & + \hbar J_{13}(b_1^\dagger b_3 + b_3^\dagger b_1), \end{aligned} \tag{2}$$

$$H_{\mathrm{int}} = \hbar\sum_{j=1}^{3} g_j(b_j a^\dagger + b_j^\dagger a), \tag{3}$$

where $a^\dagger$ and $b_j^\dagger$ are creation operators for cavity photons and excitation quanta of the jth qubit in the array, respectively. $H_{\rm cav}$ is the Hamiltonian for the 7.116 GHz waveguide cavity, which couples dispersively to each qubit in the transmon array with strength g_j, as described by $H_{\rm int}$. The array itself is described by $H_{\rm array}$: each transmon is a weakly anharmonic oscillator with $|0\rangle \rightarrow |1\rangle$ transition frequency ω_j and (negative) anharmonicity α_j. The three-qubit system is effectively an array of lattice sites on which particles—the transmon excitation quanta—can hop with nearest-neighbor tunneling strength $\hbar J$, and next-nearest-neighbor tunneling $\hbar J_{13}$ (set primarily by the capacitive coupling [35]), with $J_{13} \ll J$. In this language the negative anharmonicity of the transmon gives rise to an attractive pairwise interaction between these particles, since distributing a pair of excitations among two identical transmons takes an energy α more than lumping the quanta together on the same qubit. It is this combination of tunneling and on-site interaction which realizes the canonical 1D Bose-Hubbard Hamiltonian [21].

Since the Bose-Hubbard Hamiltonian conserves the total particle number, eigenstates of the three-qubit array can be grouped into manifolds characterized by this quantum number. In our experiment, we work with the zero, one, and two-particle manifolds, comprising, respectively, one, three, and six states. We denote the zero-particle state by $|G\rangle$, the single-particle states by $\{|E_i\rangle, i \in [1,3]\}$, and the two-particle states by $\{|F_j\rangle, j \in [1,6]\}$, with an increasing subscript value indicating higher-energy states. Because of the dispersive interaction between qubits and the cavity, a reflected microwave signal near the cavity resonance frequency acquires a phase shift dependent on the state of the array. Amplification of the readout signal via a Josephson parametric amplifier [36] and subsequent higher-temperature electronics allows for measurement of the signal phase and hence the array state.

Using this dispersive readout, we first characterize the system by spectroscopically probing its energy levels as the edge qubit frequencies are tuned down via external magnetic flux. As shown in Fig. 1, our measurement of the system's one- and two-particle energy states agrees well with predictions based on the attractive 1D Bose-Hubbard Hamiltonian. The extracted parameters are $\omega_1/2\pi = 5.074$ GHz, $\omega_2/2\pi = 4.892$ GHz, $\omega_3/2\pi = 5.165$ GHz, $J/2\pi = 0.177$ GHz, and $J_{13}/2\pi = 0.026$ GHz, all to within ± 0.003 GHz. The cavity-qubit coupling $g_1/2\pi = 149 \pm 7$ MHz, $g_2/2\pi = 264 \pm 7$ MHz, $g_3/2\pi = 155 \pm 7$ MHz, and qubit anharmonicities $\alpha_{1,3}/2\pi = -214 \pm 1$ MHz, $\alpha_2/2\pi = -240 \pm 1$ MHz, were calibrated independently. While at zero applied flux the qubits are relatively well separated in frequency, as the edge qubits are tuned down towards the middle qubit, avoided crossings become apparent, showcasing the coupling between the qubits. Our system lies in the parameter regime where the competing tunneling ($J/2\pi \sim 180$ MHz) and on-site interactions ($\alpha/2\pi \sim -220$ MHz) have nearly equal strength.

At an external field corresponding to 10 mA in the bias coil, the individual qubit frequencies approximately

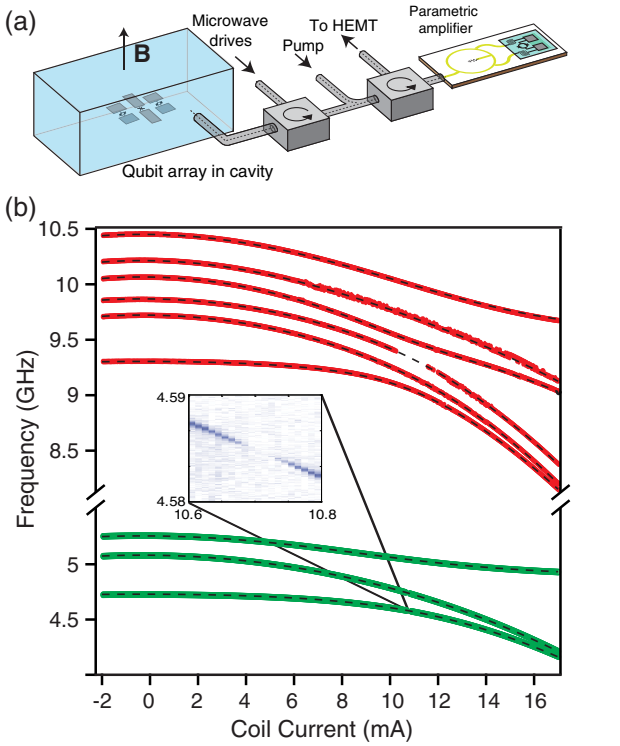

FIG. 1 (color online). (a) A schematic (not to scale) of the experimental setup described in the text. (b) Spectroscopically measured eigenfrequencies of the one- and two-particle states of the array as a function of current through the external bias coil. For a given current, the flux through the two SQUIDs in the array differs by 2.5%; 17 mA roughly corresponds to a quarter of a flux quantum. Solid lines denote measured frequencies with fits to the 1D Bose-Hubbard Hamiltonian shown as overlaid dashed lines. Red lines correspond to two-particle states; green lines are one-particle states. The inset shows raw data near the $|E_1\rangle$ frequency, from which the darkness of the $|G\rangle \rightarrow |E_1\rangle$ transition discussed in the text becomes apparent.

coincide—the detunings between neighboring qubits, 45 and 115 MHz, are lower than the tunneling rate J. At this bias we characterize—in the absence of engineered dissipation—the particle-loss dynamics resulting from coupling to the dissipative environment comprised of both the leaky cavity ($\kappa/2\pi = 10$ MHz) and microscopic material imperfections. A coherent microwave pulse initializes the system to the desired $|E_i\rangle$ or $|F_j\rangle$ state, after which the resulting populations are measured as a function of time. As expected, these decay dynamics fit well to a model which only includes single-particle loss events: direct transitions from the $|F_i\rangle$ states to $|G\rangle$ are suppressed, as recently observed with a single transmon qubit [37]. Examples of such decays are shown in Figs. 2(a) and 2(b), while Fig. 2(c) shows the full map of decay rates within these subspaces.

A striking feature of the natural decay dynamics is the discrepancy between decay times of different states in the same manifold. For example, $|E_1\rangle$ and $|E_2\rangle$ live for ~ 30 μs, while $|E_3\rangle$ decays much more quickly, in ~ 3 μs. This is due

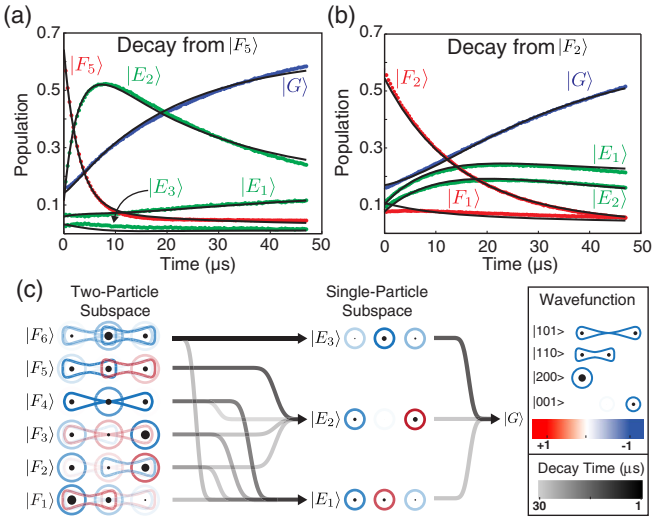

FIG. 2 (color online). (a) and (b) Examples of spontaneous decays from two-particle states to the global ground state via the one-particle subspace. In (a), $|F_5\rangle$ decays rapidly and almost entirely to $|E_2\rangle$, which then decays to $|G\rangle$, while in (b), $|F_2\rangle$ decays with roughly equal rates to $|E_1\rangle$ and $|E_2\rangle$. Overlaid black lines are obtained from fitting the decay data for all nine excited states to a single rate-equation model, as described in the Supplemental Material [39]. (c) An illustration of the natural decay pathways of the system, from the two-particle subspace on the left, through the one-particle subspace in the middle, to the zero-particle state on the right. Each black arrow represents a decay channel, with the opacity of the line indicating the rate of the transition. Darker lines indicate faster rates, as the legend shows. Also shown are representations of the eigenstate wave functions in the qubit basis. The black circle radius is proportional to the mean particle number.

to the substantially different dipole transition matrix elements that each single-particle state $|E_i\rangle$ exhibits with respect to the final state $|G\rangle$. A related consequence of these dipole moments is shown in the inset of Fig. 1, where at 10.71 mA, $|E_1\rangle$ goes fully dark, i.e., becomes impossible to excite via a coherent microwave pulse. Under only Purcell decay—in the absence of material losses in the system—such a dark state would live indefinitely, making it attractive for shelving an excitation if it could be readily prepared. We will return to the preparation of these dark states as one application of our bath engineering protocol, which we now discuss.

By altering the quantum noise spectrum of the bath interacting with the Bose-Hubbard chain, we can modify the system decay dynamics. In our cooling protocol, this alteration takes the form of an additional microwave drive incident on the cavity, red detuned from the cavity resonance by an amount Δ_c, as illustrated in Fig. 3(a) for the $|E_2\rangle$ to $|E_1\rangle$ transition. This induces quantum photon shot noise whose spectral density peaks at frequency $|\Delta_c|$ [38]. When $\hbar\Delta_c$ matches the energy difference between the array's initial state $|i\rangle$ and a lower eigenstate $|f\rangle$, the emission of a photon at the cavity's resonance frequency mediates a so-called cooling transition from $|i\rangle$ to $|f\rangle$. The energy gained from the cooling transition augments the incident photon energy to allow emission on resonance. Similarly, a blue-detuned drive induces heating transitions to array states of higher energy. The rate for these processes will depend on both the Raman-transition matrix element between the initial and final array states and on the incident photon flux. The transition rate increases with photon flux up to a value of $\sim\kappa$, saturating there as the dissipative process requires the emission of a photon by the cavity. Since κ is much larger than most of the natural decay rates, this technique is well suited to driving otherwise inaccessible particle-number-conserving transitions in our system. More details on the cooling protocol can be found in [39].

To characterize the cooling dynamics, we initialize the system into an $|E_i\rangle$ or $|F_j\rangle$ eigenstate and subsequently apply a cooling drive for a variable time and measure the state of the array. Cooling rates are extracted via a fit to a model similar to that used for the natural decays, with additional parameters to capture the induced intramanifold transitions. Because the cavity's density of states exhibits a Lorentzian profile with width κ, so will the transition rate as a function of cooling drive frequency, as shown for the $|E_2\rangle$ to $|E_1\rangle$ transition in Fig. 3(c).

For incident powers which cool at a rate $\Gamma_{i\to j}$ much lower than κ, a Fermi Golden Rule calculation [39] shows that

$$\Gamma_{i\to f} \propto P_{\mathrm{in}}|M_{if}|^2 \frac{\kappa}{(\omega_i-\omega_f+\Delta_c)^2+(\kappa/2)^2}, \qquad (4)$$

where P_{in} is the incident cooling drive power and M_{if} the matrix element connecting the states $|i\rangle$, $|f\rangle$ of the cooling operator [39] which describes the effect of the dissipative bath; in other words, M_{if} quantifies the coupling between the states $|i\rangle$ and $|f\rangle$ indirectly via the cross-Kerr terms that couple the qubits with cavity. The predicted linear scaling of the peak Γ with P_{in} is shown in the inset of Fig. 3(c) for the $|E_2\rangle \to |E_1\rangle$ transition. $|M_{ij}|$ provides a measure of the efficacy of each transition; we map out this value for each pair of eigenstates, showing the results in Fig. 3(e).

In most cases, applying a drive whose frequency is targeted to cool $|i\rangle$ to $|f\rangle$ has no effect on the decay dynamics of the other states, as most cooling drive frequencies are spaced apart by more than several κ. However, when multiple cooling frequencies are separated by less than κ, a single drive can give rise to a so-called *cascaded cooling* effect, whereby multiple cooling transitions happen in sequence. In our system, for example, the $|F_3\rangle \to |F_2\rangle$ and the $|F_2\rangle \to |F_1\rangle$ transitions are separated by only 17 MHz, so a single tone can cause the system to cascade from $|F_3\rangle$ to $|F_1\rangle$ via the intermediate state $|F_2\rangle$, as shown in Fig. 3(d). In the specific example shown, since the cooling matrix element between $|F_3\rangle$ and $|F_2\rangle$ is substantially lower than that of $|F_2\rangle$ and $|F_1\rangle$ ($|M_{21}| \sim 5|M_{32}|$), we cooled with the drive frequency tuned to the $|F_3\rangle \to |F_2\rangle$ transition; this achieved approximately equal cooling rates from $|F_3\rangle$ to $|F_2\rangle$ and $|F_2\rangle$ to $|F_1\rangle$. Cascaded cooling sequences could be useful in larger many-qubit systems with manifolds containing several closely spaced eigenstates (see [39] for details).

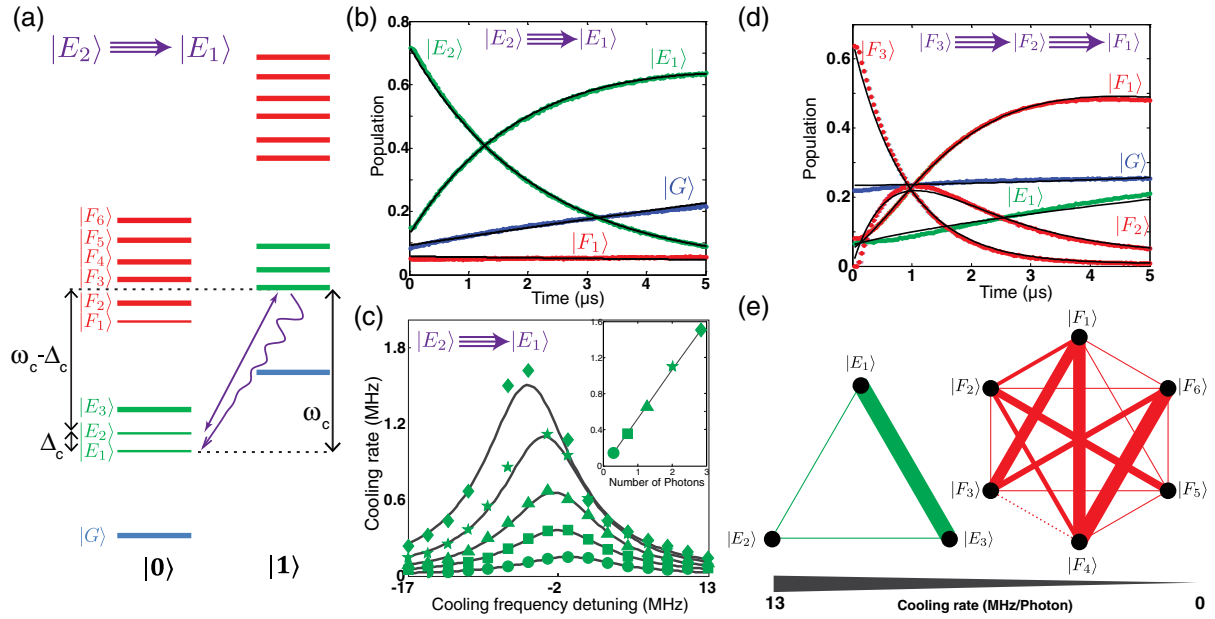

FIG. 3 (color online). (a) An approximate representation of the eigenstates of the array-cavity system; states in the left-hand (right-hand) column contain zero (one) cavity photons. In this picture, our cooling process can be understood qualitatively as follows (taking $|E_2\rangle \to |E_1\rangle$) as an example: the cooling drive at frequency $\omega_c - \Delta_c$ induces a transition from $|E_2\rangle|0\rangle$ to $|E_1\rangle|1\rangle$, where the second ket indicates the cavity photon number. The cavity state $|1\rangle$ decays via photon emission, leaving the system in the state $|E_1\rangle|0\rangle$, as desired. (b) Example of cooling from $|E_2\rangle \to |E_1\rangle$ at an incident power corresponding to 1.3 drive photons in the cavity. (c) The cooling rate versus drive frequency is Lorentzian, centered around $\omega_c - (E_2 - E_1)$, with a linewidth roughly κ. As the drive power is increased, the Lorentzian peak shifts due to a Stark shift of the relevant transition frequency. The inset shows that in the regime where the cooling rate is much lower than κ, the rate scales linearly with incident power. (d) Example of cascaded cooling, where the system is cooled from $|F_3\rangle$ to $|F_1\rangle$ via the intermediate state $|F_2\rangle$. (e) Connected graphs representing the measured cooling rates per photon in the linear regime for the one- (left-) and two- (right-)particle subspaces, with the width of the line indicating the rate of the corresponding transition. The dispersive shifts for the $|F_3\rangle$ and $|F_4\rangle$ states are almost identical, so they cannot be distinguished by our measurement. We thus do not measure cooling from $|F_4\rangle$ to $|F_3\rangle$.

The transitions $|G\rangle \to |E_1\rangle$, $|G\rangle \to |E_2\rangle$, and $|E_i\rangle \to |F_1\rangle$ do not interact strongly with the electromagnetic environment of the cavity on account of the symmetry of the states; this decoupling is responsible for their relatively long lifetimes. Correspondingly, however, it is difficult to coherently initialize these states via direct transitions, but our cooling scheme affords their efficient preparation. To illustrate this, consider the $|G\rangle \to |E_1\rangle$ transition, which as shown in Fig. 1, is at its darkest at a flux bias of 10.71 mA. At this bias point, we use the Raman cooling protocol to prepare $|E_1\rangle$ indirectly via the $|E_3\rangle \to |E_1\rangle$ cooling transition (data not shown). Further, by combining coherent drives with Raman cooling, we stabilize $|E_1\rangle$ indefinitely against particle loss. As the first part of Fig. 4 illustrates, this is done by coherently driving the $|G\rangle$ to $|E_3\rangle$ transition with a Rabi frequency of 7 MHz while applying a drive to cool the $|E_3\rangle \to |E_1\rangle$ transition at a rate of 3 MHz. We next use $|E_1\rangle$ as a stepping stone to stabilize the two-particle ground state $|F_1\rangle$, as shown in the lower part of Fig. 4. To accomplish this we add two additional drives, an extra coherent drive from $|E_1\rangle \to |F_4\rangle$ with a Rabi frequency of 7 MHz, and a cooling drive from $|F_4\rangle \to |F_1\rangle$ with a rate of approximately 3 MHz. Observed fidelities, while inline with a rate matrix calculation, are primarily limited by the spurious thermal

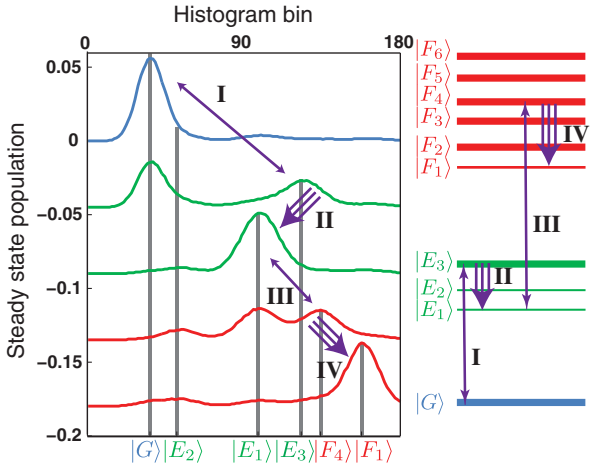

FIG. 4 (color online). Steady state population at the different stages of the persistent stabilization scheme of the two particle ground state $|F_1\rangle$. The top trace shows the thermal equilibrium population, where 78% of the population is in $|G\rangle$. In each subsequent trace a further drive is added: first a coherent drive $|G\rangle \to |E_3\rangle$ (I), then cooling from $|E_3\rangle \to |E_1\rangle$ (II), coherent drive from $|E_1\rangle \to |F_4\rangle$ (III), and finally a cooling drive from $|F_4\rangle \to |F_1\rangle$ (IV). At the end, 67% of the population is in the desired state, $|F_1\rangle$. $|F_4\rangle$ contains the bulk, 13%, of the residual population. Single-particle ($|E_1\rangle$) stabilization achieves a population of 80% (data not shown).

population of dark states, which can be reduced by additional cooling tones. This initialization and maintenance of the array in the ground state of a specific particle-number manifold will be a valuable resource for a hardware simulator.

In conclusion, we have realized a three-qubit transmon array and spectroscopically verified that it obeys an attractive 1D Bose-Hubbard Hamiltonian up to the ten lowest-lying eigenstates, highlighting the use of circuit QED in simulating otherwise challenging quantum systems. Our developed cooling and stabilization protocols, based on quantum bath engineering—a well-studied phenomenon in quantum optics—afford effective control over this solid state system. The capabilities demonstrated here —engineering decay dynamics and stabilizing particular eigenstates—show that dissipation engineering can be a valuable tool as superconducting circuits scale up in complexity to complement simulators based on cold atoms and trapped ions.

We thank F. Marquardt for motivating this line of research and acknowledge helpful discussions with U. Vool. V. V. R. acknowledges funding via a NSF graduate student fellowship. Financial support for ongoing quantum circuit development was provided by AFOSR FA9550-12-1-0378 and the current experiment was conducted under a DOE Laboratory Directed Research and Development grant. Funding for theory support is acknowledged from NSF DMR-1301798 and ARO W911NF1410011.

*shayhh@berkeley.edu

[1] B. Kraus, H. P. Büchler, S. Diehl, A. Kantian, A. Micheli, and P. Zoller, Phys. Rev. A **78**, 042307 (2008).
[2] F. Verstraete, M. M. Wolf, and J. Ignacio Cirac, Nat. Phys. **5**, 633 (2009).
[3] K. W. Murch, U. Vool, D. Zhou, S. J. Weber, S. M. Girvin, and I. Siddiqi, Phys. Rev. Lett. **109**, 183602 (2012).
[4] S. Shankar, M. Hatridge, Z. Leghtas, K. M. Sliwa, A. Narla, U. Vool, S. M. Girvin, L. Frunzio, M. Mirrahimi, and M. H. Devoret, Nature (London) **504**, 419 (2013).
[5] K. Geerlings, Z. Leghtas, I. M. Pop, S. Shankar, L. Frunzio, R. J. Schoelkopf, M. Mirrahimi, and M. H. Devoret, Phys. Rev. Lett. **110**, 120501 (2013).
[6] E. Kapit, J. T. Chalker, and S. H. Simon, Phys. Rev. A **91**, 062324 (2015).
[7] J. D. Teufel, T. Donner, D. Li, J. W. Harlow, M. S. Allman, K. Cicak, A. J. Sirois, J. D. Whittaker, K. W. Lehnert, and R. W. Simmonds, Nature (London) **475**, 359 (2011).
[8] F. Massel, S. U. Cho, J.-M. Pirkkalainen, P. J. Hakonen, T. T. Heikkilä, and M. A. Sillanpää, Nat. Commun. **3**, 987 (2012).
[9] B. Abdo, K. Sliwa, F. Schackert, N. Bergeal, M. Hatridge, L. Frunzio, A. D. Stone, and M. Devoret, Phys. Rev. Lett. **110**, 173902 (2013).
[10] T. Palomaki, J. Harlow, J. Teufel, R. Simmonds, and K. Lehnert, Nature (London) **495**, 210 (2013).
[11] R. Andrews, R. Peterson, T. Purdy, K. Cicak, C. Simmonds, R. W. Regal, and K. Lehnert, Nat. Phys. **10**, 321 (2014).
[12] N. Bergeal, F. Schackert, M. Metcalfe, L. Frunzio, D. Prober, R. J. Schoelkopf, S. M. Girvin, and M. Devoret, Nature (London) **465**, 64 (2010).
[13] M. A. Castellanos-Beltran, K. D. Irwin, G. C. Hilton, L. R. Vale, and K. W. Lehnert, Nat. Phys. **4**, 929 (2008).
[14] F. Massel, T. T. Heikkilä, J.-M. Pirkkalainen, S. U. Cho, H. Saloniemi, P. J. Hakonen, and M. A. Sillanpää, Nature (London) **480**, 351 (2011).
[15] J. Klaers, J. Schmitt, F. Vewinger, and M. Weitz, Nature (London) **468**, 545 (2010).
[16] D. Marcos, A. Tomadin, S. Diehl, and P. Rabl, New J. Phys. **14**, 055005 (2012).
[17] C. Aron, M. Kulkarni, and H. E. Türeci, Phys. Rev. A **90**, 062305 (2014).
[18] C. Aron, M. Kulkarni, and H. E. Türeci, arXiv:1412.8477.
[19] J. F. Poyatos, J. I. Cirac, and P. Zoller, Phys. Rev. Lett. **77**, 4728 (1996).
[20] C. J. Myatt, B. E. King, Q. A. Turchette, C. A. Sackett, D. Kielpinski, W. M. Itano, C. Monroe, and D. J. Wineland, Nature (London) **403**, 269 (2000).
[21] M. P. A. Fisher, P. B. Weichman, G. Grinstein, and D. S. Fisher, Phys. Rev. B **40**, 546 (1989).
[22] M. Greiner, O. Mandel, T. Esslinger, and T. W. Hansch, and I. Bloch, Nature (London) **415**, 39 (2002).
[23] T. Stöferle, H. Moritz, C. Schori, M. Köhl, and T. Esslinger, Phys. Rev. Lett. **92**, 130403 (2004).
[24] I. Bloch, J. Dalibard, and W. Zwerger, Rev. Mod. Phys. **80**, 885 (2008).
[25] P. Buonsante, V. Penna, and A. Vezzani, Phys. Rev. A **72**, 043620 (2005).
[26] P. Buonsante, V. Penna, and A. Vezzani, Phys. Rev. A **82**, 043615 (2010).
[27] M. W. Jack and M. Yamashita, Phys. Rev. A **71**, 023610 (2005).
[28] A. A. Gangat, I. P. McCulloch, and G. J. Milburn, Phys. Rev. X **3**, 031009 (2013).
[29] M. Hafezi, P. Adhikari, and J. M. Taylor, arXiv:1405.5821 [Phys. Rev. B (to be published)].
[30] R. Landig, F. Brennecke, R. Mottl, T. Donner, and T. Esslinger, Nat. Commun. **6**, 7046 (2015).
[31] R. Barends, L. Lamata, J. Kelly, L. Garcia-Alvarez, A. G. Fowler, A. Megrant, E. Jeffrey, T. C. White, D. Sank, J. Y. Mutus *et al.*, Nat. Commun. **6**, 7654 (2015).
[32] J. Koch, T. M. Yu, J. Gambetta, A. A. Houck, D. I. Schuster, J. Majer, A. Blais, M. H. Devoret, S. M. Girvin, and R. J. Schoelkopf, Phys. Rev. A **76**, 042319 (2007).
[33] A. Wallraff, D. I. Schuster, A. Blais, L. Frunzio, J. Majer, M. H. Devoret, S. M. Girvin, and R. J. Schoelkopf, Phys. Rev. Lett. **95**, 060501 (2005).
[34] H. Paik, D. I. Schuster, L. S. Bishop, G. Kirchmair, G. Catelani, A. P. Sears, B. R. Johnson, M. J. Reagor, L. Frunzio, L. I. Glazman *et al.*, Phys. Rev. Lett. **107**, 240501 (2011).
[35] O. Viehmann, J. von Delft, and F. Marquardt, Phys. Rev. Lett. **110**, 030601 (2013).
[36] M. Hatridge, R. Vijay, D. H. Slichter, J. Clarke, and I. Siddiqi, Phys. Rev. B **83**, 134501 (2011).
[37] M. J. Peterer, S. J. Bader, X. Jin, F. Yan, A. Kamal, T. J. Gudmundsen, P. J. Leek, T. P. Orlando, W. D. Oliver, and S. Gustavsson, Phys. Rev. Lett. **114**, 010501 (2015).
[38] A. A. Clerk, M. H. Devoret, S. M. Girvin, F. Marquardt, and R. J. Schoelkopf, Rev. Mod. Phys. **82**, 1155 (2010).
[39] See Supplemental Material at http://link.aps.org/supplemental/10.1103/PhysRevLett.115.240501 for the theoretical model and additional experimental details and results.